Mauro Manetti, Marco Morandini, Paolo Mantegazza, Roberto Biasi, Daniele Gallieni and Armando Riccardi, "Experimental validation of a numerical model for non-contact, massively actuated deformable adaptive mirrors", Proc. SPIE 7736, 77363W (2010);
http://dx.doi.org/doi:10.1117/12.856913

Experimental validation of a numerical model for non contact, massively actuated, deformable adaptive mirrors

Mauro Manetti[a], Marco Morandini[a], Paolo Mantegazza[a],
Roberto Biasi[b], Daniele Gallieni[c], Armando Riccardi[d]

[a]Politecnico di Milano, Dip. Ing. Aerospaziale, via La Masa 34 , 20156 Milano, Italy;
[b]Microgate srl, Via Stradivari 4, 39100 Bolzano, ITALY;
[c]ADS International srl, Via Roma 87, 23868 Valmadrera (LC), ITALY;
[d]INAF, Osservatorio Astrofisico di Arcetri, Largo E. Fermi 5, 50125 Firenze, Italy.

ABSTRACT

The validation of the multidisciplinary model of a deformable, massively actuated adaptive mirror is presented. The related experimental correlations are focused on an adaptive shell with 45 non contacting voice coils actuated points, dubbed P45, that was developed as an engineering verification prototype for the LBT adaptive secondary mirrors. A description of the multi physics model is followed by the results obtained simulating actual experimental tests and by their correlation with the related true measures. The significance of various modeling details and their impact on the correlation is discussed. The results show a remarkable match between numerical and experimental data.

1. INTRODUCTION

A fundamental step in adaptive optics evolution has been the introduction of secondary deformable mirrors with non contact voice-coil actuators, co-located with capacitive position sensors.[1] An implementation of such a design has already proven its effectiveness on the existing Multiple Mirror Telescope[2] (MMT) and a similar, close to operation adaptive system can be found on the Large Binocular Telescope[3](LBT). The same technology will be exploited by the Very Large Telescope[4] (VLT) and the Giant Magellan Telescope[5] (GMT); a possible application of the same technology is under evaluation for the M4 unit of the European Extremely Large Telescope[6] (E-ELT), where the number of controlled points could exceed 6000[7].[8]

The design and analysis of non contact, voice coil motor massively actuated, deformable adaptive mirrors requires a multidisciplinary approach encompassing: deformable structures, fluid dynamics and control systems. Such a task can be pursued by exploiting sufficiently detailed numerical models, usable in a comprehensive and thoroughly manner for all of the design, installation and operational phases. Within such a framework experimental validations are often required to achieve full confidence in the tools at hand.

This work presents the results obtained for the validation process of a detailed simulation tool, entailing an adaptive specimen with 45 actuation points, dubbed P45, that was developed as an engineering prototype for the LBT adaptive secondary mirrors[3] (see Fig. 1). This is far from the many thousands to be used in actual applications, e.g. in the E-ELT adaptive M4. Nonetheless, it is adequate to point out all of the critical design and operational aspects. A description of the multi physics model is presented, followed by the results obtained by simulating actual tests on the specimen and their correlation with true measurements. The significance of various modeling details and their effect on the correlation is discussed. Among them a thorough consideration is given to: imprecise co-location, different fluid dynamic models, sensor-actuation noises and quantization effect, compensation filters and computational delays, saturations, feed forward control identification. The remarkable match between numerical and experimental results allows a confident use of the available simulation tools within medium-high fidelity design simulations of any actual adaptive mirror developed using the presented modeling technology.

Further author information: (Send correspondence to Mauro Manetti)
Mauro Manetti: E-mail: manetti@aero.polimi.it, Telephone: +39 02 2399 8365

Figure 1: P45 prototype.

2. STRUCTURAL MODEL

The adaptive prototype here modeled involves (see Fig. 2) its deformable shell, a reference structure, the air in which it is embedded and its control system.

For a flexible and versatile description of the structural response of the whole system a linear finite element (FE) model, with n_g degrees of freedom, has been set up through the following matrix equation:

$$\mathbf{M}_g\ddot{\mathbf{x}} + \mathbf{K}_g\mathbf{x} = \mathbf{B}_x\left(\mathbf{f}_a^c + \mathbf{f}^d\right) \tag{1}$$

where $\mathbf{M}_g$, and $\mathbf{K}_g$ are the $(n_g \times n_g)$ mass and stiffness matrix, $\mathbf{f}_a^c$ and $\mathbf{f}^d$ the control and disturbance force vectors, reported at the n_a actuation points, $\mathbf{B}_x$ the force influence $(n_g \times n_a)$ matrix. Given the high modeling accuracy and the huge number of simulations required the direct use of a FE model (1), possibly coupled with a finely matched computational fluid dynamic description, can be exceedingly expensive. So a reduced model is required for low up to high fidelity "fluidoservoelastic" simulations.

To obtain a meaningful performance evaluation any reduced structural model must guarantee a good description of the structural dynamics within the band of interest and an exact recovery of the static response at the controlled points. In such a view the preferred condensation scheme will be based on the use of normal vibration modes. So the physical nodal degrees of freedom are expressed as:

$$\mathbf{x} = \mathbf{X}_g\mathbf{q} \tag{2}$$

where $\mathbf{q}$ is the chosen set of n_m generalized modal coordinates and $\mathbf{X}_g$ is the $(n_g \times n_m)$ modal shape matrix. Assuming a unit modal mass normalization the uncoupled equation of motion of the i^{th} mode is:

$$\ddot{q}_i + 2\xi_i\omega_i\dot{q}_i + \omega_i^2 q_i = f_{m_i}^c + f_{m_i}^d, \tag{3}$$

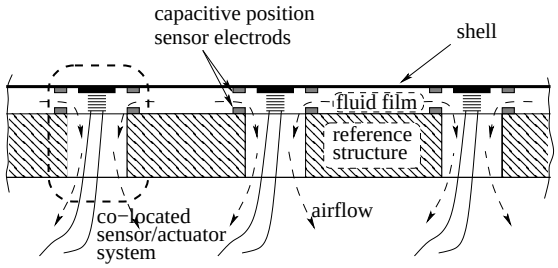

Figure 2: Mirror shell and reference structure section.

where q_i is the modal degree of freedom, ω_i, ξ_i are its natural frequency and damping coefficient. The modal control and disturbance force $(n_m \times 1)$ vectors, f_m^c and f_m^d respectively, are given by

$$\mathbf{f}_m^c = \mathbf{X}^T \mathrm{sat}(\mathbf{f}_a^c) \qquad \mathbf{f}_m^d = \mathbf{X}^T \mathbf{f}^d \tag{4}$$

where the element (i, j) of the $(n_a \times n_m)$ condensed mode shape matrix $\mathbf{X} = \mathbf{B}_x^T \mathbf{X}_g$ represents the displacement of the i^{th} actuator associated to the j^{th} normal mode and sat() accounts for possible actuators saturation.

Even if a relatively small number of modes could be sufficient for an acceptable approximation of the mirror dynamics, the need to correctly and precisely represent complex shapes imposes to use a number of modes at least equal to the number of actuators, significantly higher eventually, e.g. to verify that simulations are not affected by possible spillover effects.

Since a truncated set of normal modes cannot guarantee the exact determination of the controlled displacements at a steady state position, the exact static response can be recovered through a static residualization of the higher frequency modes response, whose dynamics is not accounted for in (3). From a general point of view such a recovery makes available a dynamically residualized model[9] that adequately recovers both the poles and the zeros of interest.[10] A precise static recovery affords a better evaluation of the actuator forces, so allowing to better check for possible saturations and design limitations.

In such a view a viable calculation of the displacement $\mathbf{s}$ at the actuators is given by:

$$\mathbf{s} = \mathbf{X}\mathbf{q} + \left(\mathbf{K}^{-1} - \mathbf{X}[\diagdown \boldsymbol{\omega}^2 \diagup]^{-1}\mathbf{X}^T\right)\left(\mathbf{f}_a^c + \mathbf{f}^d\right) \tag{5}$$

where $\mathbf{K}$ represents the $(n_a \times n_a)$ stiffness matrix condensed at the actuation points.

3. ACTUATORS AND SENSORS

The sensor-actuation units are based on non contact voice coil motors and capacitive sensors[11].[12] The actuator forces and measured positions are not exactly co-located. An electromagnetic model of the force would show both a couple and force vector acting on the permanent magnet attached to the mirror. The resulting couple vector has likely a negligible value, while the almost in plane force components have a minor effect on the mirror deformation because of the mounting restrains. The mirror shape is controlled in closed loop, so the actuator non co-location can be seen has a correctable disturbance. For this reason it is assumed that control forces can be approximated as point wise and normal to the mirror.

The actuators dynamics can be suitably approximated by an uncoupled, up to second order model, whose state space form is:

$$\dot{\mathbf{x}}_f = -[\diagdown \mathbf{A}_f \diagup]\mathbf{x}_f + [\diagdown \mathbf{B}_f \diagup]\mathbf{f}^c \qquad \mathbf{f}_a^c = [\diagdown \mathbf{C}_{\boldsymbol{f}} \diagup]\mathbf{x}_f, \tag{6}$$

where $\mathbf{f}^c$ represents the $(n_a \times 1)$ required control forces vector and the matrices $[\diagdown \mathbf{A}_f \diagup]$ $(2 \times 2$ block) and $[\diagdown \mathbf{C}_{\boldsymbol{f}} \diagup]$ $(1 \times 2$ block) are $(2n_a \times 2n_a)$ block diagonal matrices, while $[\diagdown \mathbf{C}_{\boldsymbol{f}} \diagup]$ $(2 \times 1$ block) is a $(2n_a \times n_a)$ block diagonal matrix.

A point wise co-located measure can be assumed for the capacitive position sensors just like as for the actuator forces. Such a model is quite usable but somewhat too crude for high fidelity simulations. The non co-location of sensors can be taken in due account by evaluating a motion dependent variable capacitance. It is easy to understand that the non co-location effect can become significant when sufficiently complex spatial shapes are commanded. The simulation of this effect allows a further accurate check of the real system stability, a more realistic prediction of the required control forces and a better estimate of the identified static feedforward matrix (see Sec. 4 and 5).

The real capacitance of each sensor is a non linear function of the local mirror motion:

$$\mathbf{C}_{mes} = \mathbf{C}_{mes}(\mathbf{x}_{nc}) \tag{7}$$

where $\mathbf{x}_{nc}$ is the function giving the transverse displacements of the capacitors plates. On the base of the non co-located measured capacitance the sensor dynamics is obtained through an up to second order approximation

$$\dot{\mathbf{x}}_p = -[\diagdown \mathbf{A}_p \diagup]\mathbf{x}_p + [\diagdown \mathbf{B}_p \diagup]\mathbf{V}_{in} \qquad \mathbf{V}_{out} = [\diagdown \mathbf{C}_p \diagup]\mathbf{x}_p, \tag{8}$$

where $\mathbf{V}_{in} = \mathbf{V}_{in}(\mathbf{C}_{mes})$ is the $(n_a \times 1)$ vector of the capacitance voltages, $\mathbf{V}_{out}$ is the $(n_a \times 1)$ vector of sensor voltage output and the block diagonal matrices are analogous to those of (6). The $(n_a \times 1)$ vector of the true measured position, $\mathbf{p}$, is then related to $\mathbf{V}_{out}$ through an appropriate function, $\mathbf{p} = \mathbf{p}(\mathbf{V}_{out})$. It should be remarked that the functions $\mathbf{C}_{mes}$ and $\mathbf{p}$ are generally non linear, so even if the sensors dynamics appear as linear their overall functionality is not.

The computation and A/D/A conversions introduce errors and delays on the control forces that are appropriately modeled in the simulation program. In fact the control forces applied during acquisition, computation and conversion time are the same as those of the previous discrete control step and not the new ones. Such a delay in the application of forces can be set as a fraction of the sampling period. Moreover sensors, actuators and A/D/A conversions introduce errors that are modeled as wide band noises and quantization errors. The program can take into account even possible measure inaccuracies linked to cross-talk effects among the control units. Such cross-talk phenomena derive from marginal electromagnetic interactions between actuators and capacitive sensors mounted on the same installation unit. In fact experimental verifications have shown a measurement error, p_{CT}^{err}, induced by the electromagnetic field generated by the actuator action, which can be described as

$$p_{CT}^{err} = \frac{C_{ct}}{s} \dot{f}_a^C, \tag{9}$$

where s is the real displacement of the actuation point and C_{ct} a constant parameter.

4. CONTROL SYSTEM

The adaptive system operative condition requires a mirror shape generator defining a reference shell deformation to compensate for optical aberrations. The adaptive mirror should correct the position of each actuation point following a tracking signal, then keeping it constant up to the next command step.

The actual P45 control forces can be split in two parts, one related to a proportional-derivative (PD) feedback control law, $\mathbf{f}_d^c$, and another related to a feedforward open loop contribution, $\mathbf{f}_f^c$:

$$\mathbf{f}^c = \mathbf{f}_d^c + \mathbf{f}_f^c \tag{10}$$

The PD control forces can be written as:

$$\mathbf{f}_d^c = [\diagdown \mathbf{G}_{p} \diagdown] (\mathbf{s}^r - \mathbf{p}) + [\diagdown \mathbf{G}_{d} \diagdown] \dot{\mathbf{p}} \tag{11}$$

where $[\diagdown \mathbf{G}_{p} \diagdown]$ and $[\diagdown \mathbf{G}_{d} \diagdown]$ are respectively the proportional and derivative diagonal $(n_a \times n_a)$ gain matrices. The shell velocity at each actuation point required in equation 11 is obtained through a Tustin digital realization of the following second order pseudo-derivator:

$$\dot{p} = \frac{s_L \omega_v^2}{(s_L + \omega_v)(s_L + \omega_v)} p \tag{12}$$

$$\tag{13}$$

where s_L is the complex Laplace parameter and ω_v must be chosen by compromising between bandwidth and noise attenuation.

The PD term alone is not adequate to provide the required control precision with a sufficient bandwidth because its gains are somewhat limited by stability considerations. The presence of any significant integral term cannot improve control performances without endangering bandwidth and stability, so the requested precision can be achieved by an appropriate feedforward only. The simplest feedforward scheme can be determined as the force needed to obtain a commanded steady state balanced position for the mirror, i.e. its static response. So the static feedforward contribution allows to reach the commanded mirror position and the PD feedback action improves dynamic performances by adding the damping that is fundamental to satisfy the bandwidth requirements, to quickly reach a steady state and to reject external disturbances. Assuming to know the true

structural stiffness matrix $\mathbf{K}^*$ condensed at the control points, the feedforward forces related to a requested mirror shape $\mathbf{s}^r$ can be expressed as:

$$\mathbf{f}_f^c = \mathbf{K}^* \mathbf{s}^r. \tag{14}$$

It is nonetheless more correct to dub the matrix $\mathbf{K}^*$ as feedforward (FF) matrix. It differs from the true condensed shell stiffness because of the presence of sensors non co-location. Moreover matrix $\mathbf{K}^*$ is not known. It is thus necessary to identify it, as described in Sec. 5.

To avoid sudden high changes of the control forces between subsequent command steps two $(1 - cos)$ shaping filters are applied to the position commands and feedforward forces.

It is important to note that the different control terms act at different frequencies. In fact the PD control action works at the higher control frequency (70-100 kHz), while the feedforward follows the lower command steps frequency (500-2000 Hz). This is a key factor for the control system, because it allows to apply a fully uncoupled high frequency control trough the PD and to introduce a fully coupled feedforward contribution at a lower frequency.

5. IDENTIFICATION

To grant a precise positioning the control strategy described in Sec. 4 relies on an experimental identification of the static feedforward matrix $\mathbf{K}^*$. This allows to intrinsically compensate imprecise co-locations and sensors/actuators static gain differences.

The on field identification of $\mathbf{K}^*$ is a kind of pre-operational training phase based on a series of well established balanced conditions, often obtained through the application of a simple preliminary proportional feedback only. In view of a least square solution a set of positions $\mathbf{p}_i$ are commanded. Once a well balanced position is reached, it is kept constant for a relatively long time computing the averages $\overline{\mathbf{p}_i}$ and $\overline{\mathbf{f}_i}^c$. After taking into account also a possible constant disturbance $\overline{\mathbf{f}}^{d*}$, one can write the following overdetermined system of equations:

$$\begin{bmatrix} \overline{\mathbf{p}}_1^T & -1 \\ \overline{\mathbf{p}}_2^T & -1 \\ \vdots & \vdots \\ \overline{\mathbf{p}}_n^T & -1 \end{bmatrix} \begin{bmatrix} \mathbf{K}^* \\ \overline{\mathbf{f}}^{d*T} \end{bmatrix} = \begin{bmatrix} \overline{\mathbf{f}}_1^{cT} \\ \overline{\mathbf{f}}_2^{cT} \\ \vdots \\ \overline{\mathbf{f}}_n^{cT} \end{bmatrix}. \tag{15}$$

The "relatively long time" required to take averaged steady positions/forces, is usually in the range of a few hundredths of a second. It is mainly determined by the square root of the measurements number needed to lower the constant measures error to within an acceptable negligible value.

The importance of correctly simulating the sensor non co-location can be seen in Fig. 3, which compares the eigenvalues of the feedforward matrix of the P45 prototype as retrieved by simulated and experimental identifications. It is possible to appreciate how this comparison points out a better correlation of the non co-located results, especially for the highest eigenvalues. So the predicted feedforward forces will be more accurate, in relations to the highest modal shapes mostly, i.e. the wavy ones, when the distributed nature of the capacitance measure is more evident.

The just explained identification process can represent a challenge from the simulation point of view because it requires the calculation of a large number of relatively long time command steps. In fact during the identification phase the single simulated command time length has to be sufficiently long, ten folds the operational commands approximately, to achieve adequate forces and positions averages. So in the case of real adaptive mirrors with thousands of actuation points the simulation of this operation can become impracticable. In order to reduce the computational time and to make the simulation feasible a simpler and more effective procedure based on the sole static response can thus be used. Once the system reaches the steady state position it is possible to neglect the time dependent terms. Moreover the feedforward contribution is null during the pre-operational phase. So the acting force can be written as

$$\overline{\mathbf{f}} = \left[\diagdown \mathbf{G}_p \diagdown \right] (\mathbf{s}^r - \overline{\mathbf{p}}) + \overline{\mathbf{f}}^{d*}, \tag{16}$$

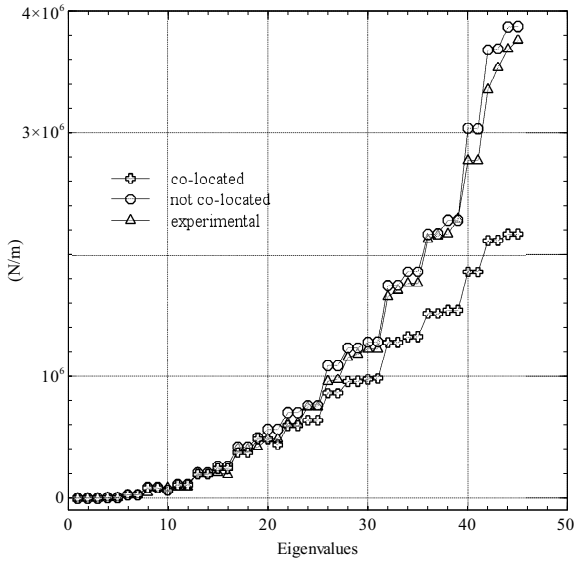

Figure 3: Comparison between the eigenvalues of three different FF matrices: experimental, numerical with co-location, numerical without co-location.

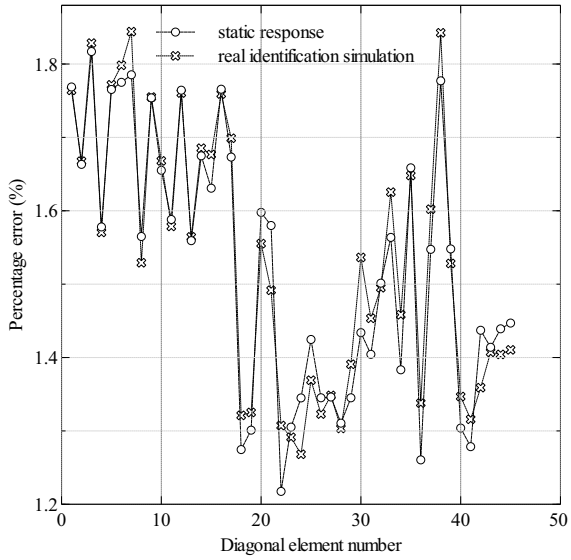

Figure 4: Percentage error of the diagonal FF matrix elements identified through: real simulation of identification process, static response approach.

while the modal static equation describing the steady behavior is

$$[\diagdown\boldsymbol{\omega}^2\diagup]\overline{\mathbf{q}} = \mathbf{X}^T\overline{\mathbf{f}} \tag{17}$$

The physical position can be gathered in two different ways, depending on the need, or not, of using a high frequency recovery

$$\overline{\mathbf{p}} = \mathbf{X}\overline{\mathbf{q}} \qquad \text{no recovery} \tag{18}$$

$$\overline{\mathbf{p}} = \mathbf{X}\overline{\mathbf{q}} + \left(\mathbf{K}^{*-1} - \mathbf{X}[\diagdown\boldsymbol{\omega}^2\diagup]^{-1}\mathbf{X}^T\right)\overline{\mathbf{f}} \qquad \text{recovery} \tag{19}$$

Now combining Eqs. 16, 17 and either 18 or 19 into a single system, it is possible to find the steady position $\overline{\mathbf{p}}$ that will be achieved for each command $\mathbf{s}^r$

$$\left(\mathbf{I} + \mathbf{X}[\diagdown\boldsymbol{\omega}^2\diagup]^{-1}\mathbf{X}^T[\diagdown\mathbf{G}_p\diagup]\right)\overline{\mathbf{p}} = \mathbf{X}[\diagdown\boldsymbol{\omega}^2\diagup]^{-1}\mathbf{X}^T\left([\diagdown\mathbf{G}_p\diagup]\mathbf{s}^{\boldsymbol{r}} + \overline{\mathbf{f}}^{d*}\right) \qquad \text{no recovery} \tag{20}$$

$$\left(\mathbf{I} + \mathbf{K}^{*-1}[\diagdown\mathbf{G}_p\diagup]\right)\overline{\mathbf{p}} = \mathbf{K}^{*-1}\left([\diagdown\mathbf{G}_p\diagup]\mathbf{s}^r + \overline{\mathbf{f}}^{d*}\right) \qquad \text{recovery} \tag{21}$$

The system is solved by carrying out a single LU factorization at the beginning of the identification process. The force $\overline{\mathbf{f}}$ is recovered afterward by simply substituting the obtained position $\overline{\mathbf{p}}$ in Eq. 16. To simulate a realistic experimental identification it is necessary to introduce the time average of noises on the steady forces and positions. In this way it is possible to recover the identified stiffness matrix without the need of any time-consuming transient simulation. Such a procedure has been verified against full transient simulations of the type used in actual operative conditions. Fig. 4 shows the diagonal element percentage error of two FF matrices of the P45, identified respectively through the simulation and the static response approach. The error has been computed with respect to the ideally correct FF matrix, which is possible to obtain in absence of noises and measurement errors. Fig. 4 demonstrates that the static response approach can afford a stiffness matrix having the same quality as that obtained through the simulation of the real identification process. The related advantage in terms of computational time and cost is very important.

6. FLUID FILM MODELS

It is here assumed that the sound emission and the mild air turbulence within which the mirror operates have a negligible effect on the positioning performances of the closed loop controlled system, the latter being attenuated

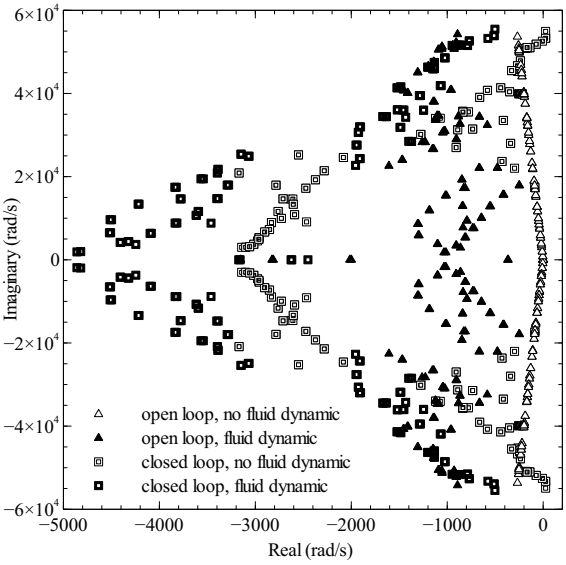

Figure 5: P45 linearized system eigenvalues, considering and neglecting fluid dynamic contributions.

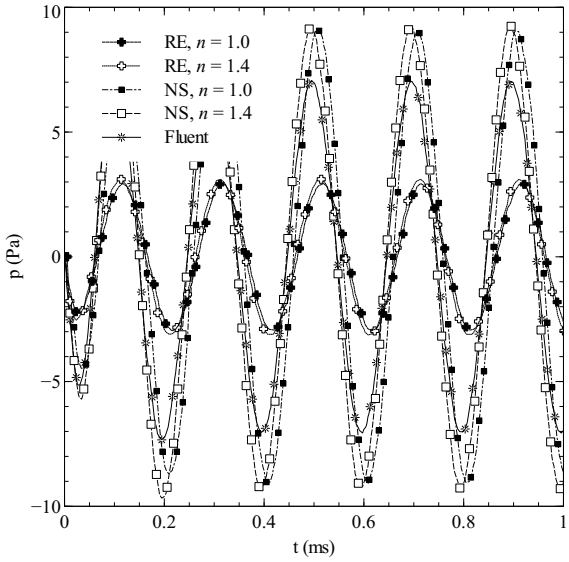

Figure 6: Comparison of a harmonic pressure history using RE-NS models and Fluent.

by feedback terms and by the external optical loop. Instead, the forces exerted by the fluid air film interposed between the shell and the reference plane can significantly affect the system response and performances. So a supposedly adequate fluid dynamic model is mandatory to correctly describe the adaptive system behavior. The need of a reliable fuild film model is confirmed by the much better correlations with test data obtained after its introduction.

The fluid film thickness between the shell and the reference backplate spans a range of $30\mu\text{m} - 120\mu\text{m}$. Its forces against the shell motions, albeit being relatively small, can significantly affect the shell stability and response. So, while it is generally conservative to design a controller discarding its influence, it is important to take it into account during advanced design phases when one wants to push performances closer to those really achievable. Just to give an example Fig. 5 shows the changes of the eigenvalues of the P45 linearized model, considering and neglecting the fluid dynamic contribution for both an open and closed loop system. It is possible to appreciate that using the actual experimental gains the simulated closed loop system without any fluid contribution would be unstable, while the real system is known to be well stable. On the other side some fluid dynamic over-damping can badly affect larger adaptive mirrors, compromising the possibility to correctly track high frequency command rate.

Such a thin fluid layer is often called a squeeze film. It is characterized by its (harmonic) squeeze number, $\sigma = (12\mu\omega_0 l_0)/(p_0^f h_0^2)$, where p_0^f and h_0 are the reference pressure and film height, μ the dynamic viscosity, l_0 a reference extension, ω_0 the shell oscillation frequency. At higher squeeze numbers the fluid forces result in being mainly elastic, while at lower ones they mostly tend to produce damping.[13] The modified squeeze film Reynolds number, $Re = (\rho_0\omega_0 h_0^2)/(\mu)$, ρ_0 being the reference fluid density, is usually very small. Flows related to very low Reynolds numbers, $Re << 1$, are often approximated through a creeping flow, using the Reynolds equation (RE). Such a model can become inadequate for squeezes at high frequency, i.e. up to many thousands of Hz, such as those to be accounted for in massively controlled mirror shells. In order to deal with such high frequencies there is the need to take into account flow inertial effects through a specialized two dimensional (2D) formulation based on non linear Navier-Stokes equations (NS). Such a general framing is summarized in the following set of equations:[14]

- either a 2D creeping flow (RE)

$$\nabla\left(\frac{\rho h^3}{12\mu}\nabla p^f\right) = \frac{\partial}{\partial t}\left(\rho h\right) \tag{22}$$

- or a 2D Navier-Stokes (NS)

$$\begin{aligned}
&\frac{\partial \rho}{\partial t} + \frac{\partial \rho u}{\partial x} + \frac{\partial \rho v}{\partial y} = 0 \\
&\rho\left(\frac{\partial u}{\partial t} + u\frac{\partial u}{\partial x} + v\frac{\partial u}{\partial y}\right) = -\frac{\partial p^f}{\partial x} + \mu\frac{\partial^2 u}{\partial z^2} \\
&\rho\left(\frac{\partial v}{\partial t} + u\frac{\partial v}{\partial x} + v\frac{\partial v}{\partial y}\right) = -\frac{\partial p^f}{\partial y} + \mu\frac{\partial^2 v}{\partial z^2}
\end{aligned} \tag{23}$$

where x and y are the mirror (mainly) in plane axes and z the normal one, u and v are the velocity components along the x and y directions and h is the flow thickness. The perfect gas state equation and the assumption of a generic polytropic relation complete the equations set

$$p^f = \rho RT \qquad p^f \rho^{-n} = const, \tag{24}$$

together with the boundary-initial conditions

$$\begin{aligned}
&p^f_(t, \partial\Omega) = p^f_{\partial\Omega} && u(t_0, \Omega) = u_{t_0} \\
&p^f(t_0, \Omega) = p^f_{t_0} && v(t_0, \Omega) = v_{t_0} \\
&T(t_0, \Omega) = T_{t_0}
\end{aligned} \tag{25}$$

where t_0 is the initial time, while Ω is the spatial domain and $\partial\Omega$ the domain boundary. The polytropic relation, i.e. $p^f \rho^{-n} = const$, is introduced as a replacement of the energy equation, and allows to consider conditions that ranges from isothermal, $n = 1$, to adiabatic, $n = 1.4$.

The validity of such an approximation for the problem at hand has been numerically verified against high fidelity fluid analyses (not "fluidoelastic"), performed by solving the complete 3D Navier-Stokes laminar equations through Fluent. Fig. 6 shows a comparison of pressure values retrieved under the P45 shell commanding a spatial wavy mirror deformation, harmonic in time with a frequency of 5 kHz. Fig. 6 is just a sample of a large set of high fidelity verifications and clearly shows the importance of taking into account inertial effects in momentum conservation for high frequency oscillations. Also the polytropic exponent becomes important to well characterize the fluid dynamic description.

The discretization of the above partial differential equations into a set of ordinary differential equations in time is carried out through a 2D node based Finite Volume discretization, with the film volume height h varying in time as imposed by the shell and backplate motions. Details about the implementation are out of the scope of this paper. The surface discretization is based on triangular meshes with up to three unknowns for each node: p^f (or ρ), ρu and ρv. The fluid film discretized equations are coupled to the structural motions through the terms h and $\dot{h}$ obtained through a modal interface between the fluid dynamic nodes and the structural modal coordinates. To maintain an appropriate energy conjugation the transpose of the very same scheme is used to compute the related generalized forces of the fluid onto the shell.

Depending on the level of fidelity desired for the design/verification simulations, the discrete "fluidoservoelastic" model obtained within the framework of this work can lead to many hundreds of thousands equations, that are solved within an explicit Runge-Kutta scheme. The use of an explicit integration might not be the best choice from a numerical point of view. Nonetheless, it is thought to be the best compromise for a hybrid digital-analogue simulation. In fact with an appropriate time step it is possible to assure a negligible numerical dissipation, an easy description of the nonlinearities related to sensors/actuators saturations and to the fluid dynamic description and an exact match of any discrete delay related to the digital implementation of the system. Note that the use of an integration scheme that introduce small, if not negligible numerical dissipation is very important, in view of the relatively small physical damping of the structural system, for the assessment of the closed-loop stability of the controlled structure.

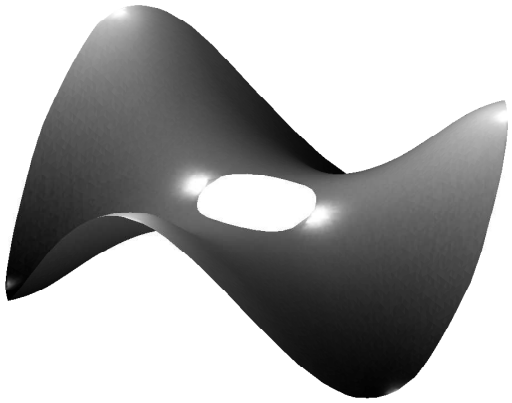

Figure 7: 6^{th} SVD right vector shape on the P45 prototype.

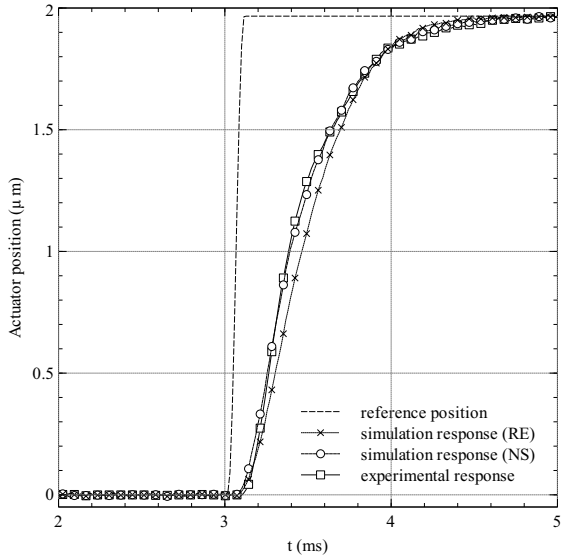

Figure 8: Response of P45 prototype to a step command (actuator 15).

7. SIMULATION RESULTS

This section presents an excerpt of the extensive results available for the correlation between numerical and experimental data. The fluid dynamic description is fundamental to reproduce the real system behavior. Both the schemes shown in Sec. 6 are able to correctly represent the low frequency fluid effects, which mainly characterize the system response, but only the improved model (NS) allows to use the real experimental gains without endangering system stability. In fact P45 stability is often linked to the system high frequency description, which, as remarked before, is affected by the inertial fluid dynamic contribution. Different feedback gains obviously lead to different transient behavior, and dynamic performances, of the system.

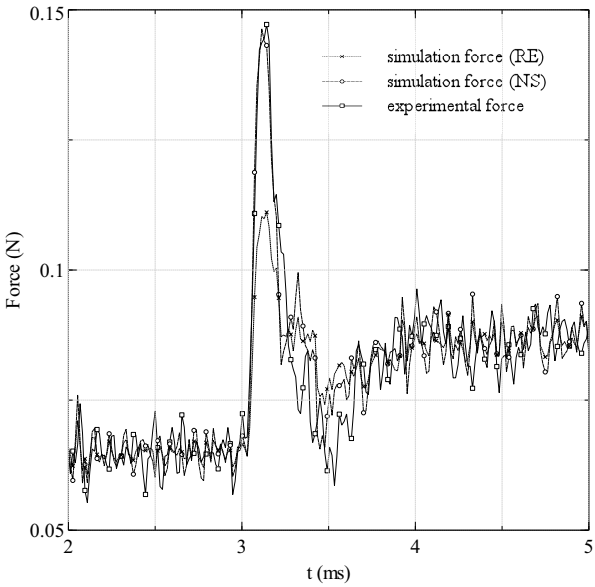

Figure 9: Control force required to track the step command on P45 prototype (actuator 18).

Figure 10: 21^{th} SVD right vector shape on the P45 prototype.

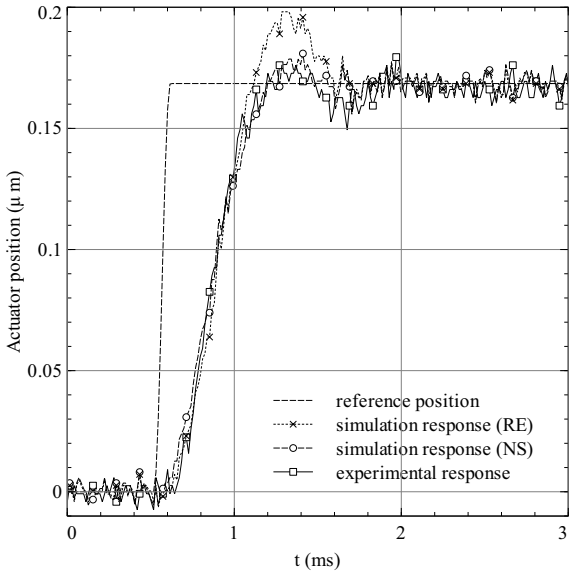

Figure 11: Response of P45 prototype to a step command (actuator 11).

Fig. 8 shows the P45 step response to the 6^{th} right vector shape of the Singular Value Decomposition (SVD) obtained from the experimentally identified FF matrix(see Fig. 7). It should be noted that the system mass matrix can be suitably approximated as being diagonal and the non co-location effects maintain the FF matrix structure relatively close to the shell stiffness. In such a view, the SVD right vector shapes end in being very similar to appropriately scaled normal modes of vibration. It is possible to appreciate the very good agreement between the numerical simulation and the experimental response. The simulation performed using the (NS) description is closer to reality because it is possible to use the real experimental controller gains, that would lead to an unstable behavior with the (RE) fluid model. The effect of the different fluid models is emphasized in Fig. 9, where it is evident that the control force during the transient phase heavily depends on the feedback gains. Of course the steady state is completely characterized by the static force required to reach a commanded position, which is fully determined by the FF matrix.

The same considerations can be done looking at Fig. 11, which shows a comparison of the P45 experimental and simulated responses to a command shaping the 21^{th} SVD right vector shape, represented in Fig 10. In this situation the system response is less damped and it is possible to appreciate the simulator capability to correctly capture the real dynamics, even in presence of an overshooting response.

The sensors non co-location effects are more remarkable in presence of a complex spatial shell deformation, e.g in Fig. 12, which emphasizes the differences between an ideal point-wise approximation and an averaged non co-located measure. Fig. 13 and Fig. 14 show the response and the control force correlation commanding the 41^{th} SVD right vector shape. It is evident how the imprecise co-location hypothesis does not affect the system response, while the non co-location description is fundamental to correctly retrieve the experimental static force values required to deform the shell. This is the reason why the identified FF matrix obtained simulating the sensors non co-location is closer to the experimental one, as pointed out in Sec. 5.

8. FINAL REMARKS

This work emphasizes the need of a comprehensive multidisciplinary approach to correctly model an adaptive mirror system, based on the non contact voice coil technology.

The simulation results show that the code allows to obtain good correlations with experimental data. Two fluid dynamic models have been implemented. The simpler scheme (RE) is capable to adequately represent

a substantial part of the system response, but shows only a gross approximation of high frequency fluid dynamic effects, strongly influencing the system stability margins. This defect has hindered the adoption of the experimental feedback gains within the simulations, so affecting the resulting system correlation performances. The problem can be fixed by taking into account the fluid dynamic inertial contribution through an improved model (NS), so that both the responses and the control forces can be predicted by numerical analysis with high accuracy.

The sensors non co-location description seems to not affect the system dynamics and its stability substantially, but it is of primary importance in obtaining realistic predictions of the FF matrix, i.e. of the static control forces required in presence of sufficiently complex spatial deformations.

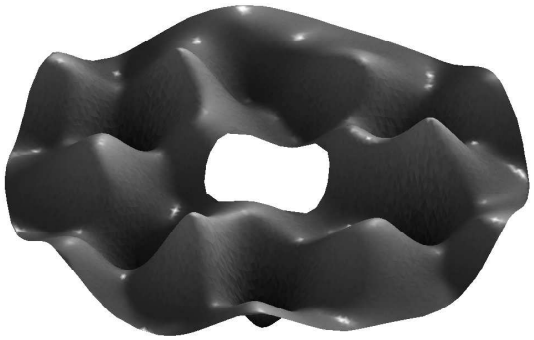

Figure 12: 41^{th} SVD right vector shape on the P45 prototype.

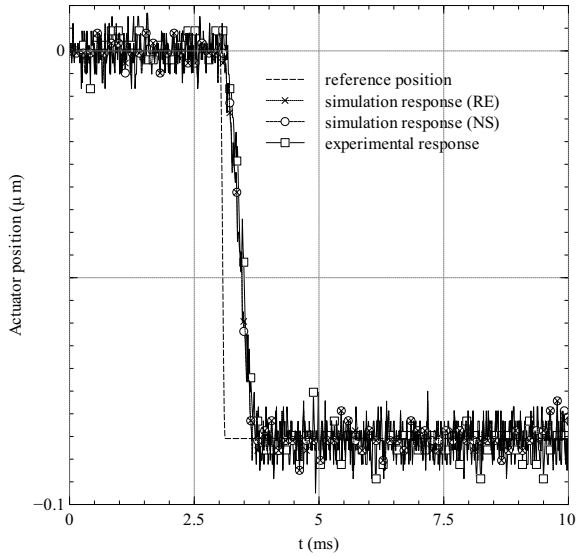

Figure 13: Response of P45 prototype to a step command (actuator 43).

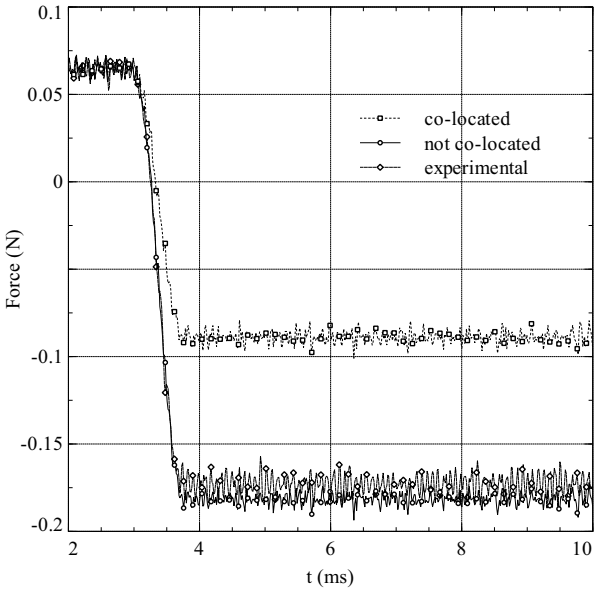

Figure 14: Sample actuator force histories computed with and without co-location hypothesis vs experimental results (41^{th} SVD shape, actuator 43).

The fidelity of the results obtained allows to consider the simulation code a valuable tool to check and develop adaptive mirror designs.

REFERENCES

[1] Salinari, P., Del Vecchio, C., and Biliotti, V., "A study of an adaptive secondary mirror," in [*Proc. ESO Conference, ICO-16 Satellite Conference, Active and Adaptive Optics*], (August 1993).

[2] Riccardi, A., Brusa, G., Del Vecchio, C., Biasi, R., Andrighettoni, M., Gallieni, D., Zocchi, F., Lloyd-Hart, M., Martin, H. M., and Wildi, F., "Adaptive secondary mirror for the 6.5-m conversion of the multiple mirror telescope," in [*Beyond Conventional Adaptive optics*], (May 2001).

[3] Riccardi, A., Brusa, G., Salinari, P., Busoni, S., Lardiere, O., Ranfagni, P., Gallieni, D., Biasi, R., Andrighettoni, M., Miller, S., and Mantegazza, P., "Adaptive secondary mirrors for the large binocular telescope," in [*Proceedings SPIE, Astronomical Adaptive Optics Systems and applications*], (August 2003).

[4] Strobele, S., Arsenault, R., Bacon, R., Biasi, R., Bonaccini-Calia, D., Downing, M., Conzelman, R., Delabre, B., Donaldson, R., Duchateau, M., Esposito, S., Fedrigo, E., Gallieni, D., Hackenberg, W., Hubin, N., Kasper, M., Kissle-Patig, M., Louarn, M. L., McDermid, R., Oberti, S., Paufique, J., Riccardi, A., Stuik, R., and Vernet, E., "The eso adaptive optics facility," in [*Proceedings SPIE, Advances in Adaptive Optics II*], (June 2006).

[5] Lloyd-Hart, M., Angel, R., Milton, N. M., Rademacher, M., and Codona, J., "Design of the adaptive optics system for gmt," in [*Proceedings SPIE, Adavances in Adaptive Optics II*], (May 2006).

[6] Gallieni, D., Tintori, M., Mantegazza, M., Anaclerio, E., Crimella, L., M. Acerboni, R. B., Angerer, G., Andrigettoni, M., Merler, A., Veronese, D., Carel, J. L., Marque, G., Molinari, E., Tresoldi, D., Toso, G., Spanò, P., Riva, M., Mazzoleni, R., Riccardi, A., Mantegazza, P., Manetti, M., Morandini, M., Vernet, E., Hubin, N., Jochum, L., Madec, P., Dimmler, M., and Koch, F., "Voice-coil technology for the E-Elt M4 adaptive unit," in [*1st International Conference on Adaptive Optics for Extremely Large Telescopes*], (2009).

[7] Strobele, S., Madec, P., N.Hubin, Stroebele, J. P. S., Soenke, C., Donaldson, R., Fedrigo, E., Oberti, S., Tordo, S., Downing, M., Kiekebusch, M., Konzelmann, R., Jost, M. D. A., Hackenberg, W., Calia, D. B., Delabre, B., Stuik, R., Biasi, R., Gallieni, D., Lazzarini, P., Lelouarn, M., and Glindeman, A., "Eso adaptive optics facility," in [*Proceedings SPIE, Adaptive Optics Systems*], (June 2008).

[8] Vernet, E., Jochum, L., Penna, P. L., Hubin, N., Muradore, R., Casalta, J., Kjelberg, I., Sinquin, J., Locre, F., Morin, P., Cousty, R., Lurcon, J., Roland, J., Crepi, B., Gabriel, E., Biasi, R., Andrighettoni, M., Gallieni, G. A. D., Mantegazza, M., Tintori, M., Molinari, E., Tresoldi, D., Toso, G., Spano, P., Riva, M., Crimi, G., Riccardi, A., Marque, G., Carel, J., and Ruch, E., "The field stabilization and adaptive optics mirrors for the european extremely large telescope," in [*Procedings SPIE, Adaptive Optics System*], (June 2008).

[9] Ghiringhelli, G. L., Lanz, M., Mantegazza, P., and Ricci, S., "Active flutter suppression techniques in aircraft wings," in [*Integrated Technology Methods and Applications in Aerospace Systems Design*], *Control and Dynamic Systems Series* **52**, 57–115, Academic Press (1992).

[10] Halim, D. and Moheimani, S. O. R., "Reducing the effect of truncation error in spatial and pointwise models of resonant systems with damping," *Mechanical System and Signal Processing* **18**, 291–315 (March 2004).

[11] Brusa-Zappellini, G., Riccardi, A., Ragland, S. D., Esposito, S., Del Vecchio, C., Fini, L., Stefanini, P., Biliotti, V., Ranfagni, P., Salinari, P., Gallieni, D., Biasi, R., Mantegazza, P., Sciocco, G., Noviello, G., , and Invernizzi, S., "Adaptive secondary p30 prototype: Laboratory results," in [*Proceedings SPIE, Adaptive Optical System Technologies*], 764–775 (September 1998).

[12] Ricci, D., Riccardi, A., and Zanotti, D., "Calibration of force actuators on an adaptive secondary prototype," *Applied Optics* **47**, 3631–3636 (2008).

[13] Bao, M. and Yang, H., "Squeeze film air damping in mems," *Sensors and Actuators A: Physical* **136**(1), 3–27 (2007).

[14] Gross, W., [*Gas Film Lubrication*], John Wiley & Sons Inc (1962).

TRANSFER OF COPYRIGHT TO SOCIETY OF PHOTO-OPTICAL INSTRUMENTATION ENGINEERS (SPIE)

Title of Paper: _____

SPIE Paper Number: (xxxx-xx) _____

Author(s): _____

This signed statement must be returned to SPIE prior to the scheduled publication of the Proceedings or Journal in which the Paper will be published. The intent of this Agreement is to protect the interests of both SPIE and authors/employers and to specify reasonable rights for both parties related to publication and reuse of the material.

The undersigned hereby assign(s) to Society of Photo-Optical Instrumentation Engineers (SPIE) copyright ownership in the above Paper, effective if and when the Paper is accepted for publication by SPIE and to the extent transferable under applicable national law. This assignment gives SPIE the right to register copyright to the Paper in its name as claimant and to publish the Paper in any print or electronic medium.

Authors, or their employers in the case of works made for hire, retain the following rights:

1. All proprietary rights other than copyright, including patent rights.
2. The right to make and distribute copies of the Paper for internal purposes.
3. The right to use the material for lecture or classroom purposes.
4. The right to prepare derivative publications based on the Paper, including books or book chapters, journal papers, and magazine articles, provided that publication of a derivative work occurs subsequent to the official date of publication by SPIE.
5. The right to post an author-prepared version or an official version (preferred version) of the published paper on an internal or external server controlled exclusively by the author/employer, provided that (a) such posting is noncommercial in nature and the paper is made available to users without charge; (b) a copyright notice and full citation appear with the paper, and (c) a link to SPIE's official online version of the abstract is provided using the DOI (Document Object Identifier) link.

   Citation format:
   Author(s), "Paper Title," Publication Title, Editors, Volume (Issue) Number, Article (or Page) Number, (Year).

   Copyright notice format:
   Copyright XXXX (year) Society of Photo-Optical Instrumentation Engineers. One print or electronic copy may be made for personal use only. Systematic reproduction and distribution, duplication of any material in this paper for a fee or for commercial purposes, or modification of the content of the paper are prohibited.

   DOI abstract link format:
   http://dx.doi.org/DOI# (*Note: The DOI can be found on the title page or online abstract page of any SPIE article.)*

If the work that forms the basis of this Paper was done under a contract with a governmental agency or other entity that retains certain rights, this Transfer of Copyright is subject to any rights that such governmental agency or other entity may have acquired.

By signing this Agreement, the authors warrant that (1) the Paper is original and has not previously been published elsewhere; (2) this work does not infringe on any copyright or other rights in any other work; (3) all necessary reproduction permissions, licenses, and clearances have been obtained; and (4) the authors own the copyright in the Paper, are authorized to transfer it, and have full power to enter into this Agreement with SPIE.

WHO SHOULD SIGN. This form must be signed by (1) at least one author who is not a U.S. Government employee and (2) the author's employer if the Paper was prepared within the scope of the author's employment or was commissioned by the employer. If not signed by all authors, the author(s) signing this Agreement represents that he/she is signing this Agreement as authorized agent for and on behalf of all the authors.

Author's signature	Print name	Date (mm/dd/yyyy)
Author's signature	Print name	Date (mm/dd/yyyy)
Authorized Employer signature	Print name Title	Date (mm/dd/yyyy)

U.S. GOVERNMENT EMPLOYMENT CERTIFICATION

A work prepared by a U.S. Government employee as part of his or her official duties is not eligible for U.S. Copyright. If all authors were U.S. Government employees when this Paper was prepared, and the authors prepared this Paper as part of their official duties, at least one author should sign below. If at least one author was not a U.S. Government employee, the work is eligible for copyright and that author should sign the Transfer of Copyright form above.

Author's signature	Print name	Date (mm/dd/yyyy)

Director of Publications, SPIE, P.O. Box 10, Bellingham, WA 98227-0010 USA
Phone: 360/676-3290 (Pacific Time) • Fax: 360/647-1445 • E-mail: copyrights@spie.org • http://SPIE.org *Revision 9 May 2011*